Ⅳ.　研究成果の刊行（平成23～25年度）に関する一覧

論文

発表者氏名	論文タイトル名	発表誌名	巻号	ページ	出版年
Otani N, Ishihara M, Nakai K, Fujita M, Wada K, Mori K	Uncooled infrared camera for the noninvasive visualization of the vascular flow in an anastomotic vessel during neurological surgery: Technical Note	Neurologia medico-chirurgica			[Epub ahead of print]
Ishihara M, Hirasawa T, Okawa S, Sato R, Urano Y, Teranishi T	The effect of surface charge of plasmonic gold nanoparticles on photoacoustic signal	Proceedings of SPIE	8943	89434D-1-8 9434D-6	2014年3月
Okawa S, Hirasawa T, Kushibiki T, Ishihara M	Reconstruction of the optical absorption coefficient from photoacoustic signals measured by scanning coaxial probe with regularization methods	Proceedings of SPIE	8943	89433W-1-8 9433W-8	2014年3月
Hirasawa T, Okawa S, Fujita M, Kushibiki T, Ishihara M	Quantification of optical attenuation coefficient based on continuous wavelet transform of photoacoustic signals measured by a focused broadband acoustic sensor	Proceedings of SPIE	8943	89435Z-1-18 9435Z-10	2014年3月
Hirasawa T, Fujita M, Okawa S, Kushibiki T, Ishihara M	Quantification of effective attenuation coefficients using continuous wavelet transform of photoacoustic signals	Applied Optics	52(35)	8562-8571	2013年12月
石原美弥	光音響信号の周波数成分が画像性能に与える影響	電気学会研究会資料光・量子デバイス研究会資料	OQD-13-047	27-29	2013年11月
Okawa S, Hirasawa T, Kushibiki T, Ishihara M	Numerical evaluation of linearized image reconstruction based on finite element method for biomedical photoacoustic	Optical Review	20(5)	442-451	2013年10月

発表者氏名	論文タイトル名	発表誌名	巻号	ページ	出版年
	imaging				
Ishihara M, Okawa S, Sato R, Hirasawa T, Teranishi T	Photoacoustic signal enhancement by localized surface plasmon of gold nanoparticles	Proceedings of the International Conference Nanomaterials: Applications and Properties	2(4)	04NABM12-1-04NABM12-3	2013年8月
堀口明男, 淺野友彦	前立腺癌に対する光音響イメージングを用いた局在診断の可能性	日本レーザー医学会誌	34(1)	19-23	2013年6月
Okawa S, Hirasawa T, Kushibiki T, Ishihara M	Reconstruction of the optical properties of inhomogeneous medium from photoacoustic signal with lp sparsity regularization	Proceedings of SPIE	8581	858135-1-858135-6	2013年3月
Hirasawa T, Fujita M, Okawa S, Kushibiki T, Ishihara M	Improvement in quantifying optical absorption coefficients based on continuous wavelet-transform by correcting distortions in temporal photoacoustic waveforms	Proceedings of SPIE	8581	85814J-1-85814J-7	2013年3月
辻田和宏	光音響イメージングの医療応用に向けて –光音響画像と超音波画像の融合–	レーザー医学会誌	33(4)	380-385	2013年1月
櫛引俊宏, 石原美弥	細胞観察のための光音響イメージング顕微鏡	レーザー医学会誌	33(4)	392-398	2013年1月
石原美弥	レーザー生体相互作用とその治療と診断への応用	光学	41(11)	548-555	2012年11月
櫛引俊宏, 平沢壮, 大川晋平, 石原美弥	3次元培養細胞観察のための光音響イメージング顕微鏡の創製	日本レーザー医学会誌	33(3)	318	2012年11月
石原美弥	光音響画像の現状	電気学会論文誌C(電子・情報・システム部門誌)	132(8)	1287-1290	2012年8月

発表者氏名	論文タイトル名	発表誌名	巻号	ページ	出版年
平沢壮, 櫛引俊宏, 藤田真敬, 石原美弥	連続ウェーブレット変換を用いた光音響信号解析による光吸収係数同定法の開発	第51回日本生体医工学会			2012年5月
石原美弥	光と超音波のハイブリッドモダリティとしての光音響画像	医学のあゆみ	240(6)	487-497	2012年2月
Hirasawa T, Ishihara M, Tsujita K, Hirota K, Irisawa K, Kitagaki M, Fujita M, Kikuchi M	Continuous wavelet-transform analysis of photoacoustic signal waveform to determine optical absorption coefficient	Proceedings of SPIE	8223	822333-1-822333-7	2012年1月
Irisawa K, Hirota K, Tsujita K, Hirasawa T, Ishihara M	Influence of laser pulse width to the photoacoustic temporal waveform and the image resolution with a solid-state excitation laser	Proceedings of SPIE	8223	82232W-1-82232W-8	2012年1月
平沢壮, 石原美弥, 藤田真敬, 北垣学, 大谷直樹, 菊地眞	光音響画像化技術の要素技術開発とシステム化:動物モデルによる性能検証	Optics and Photonics Japan 2011		P65-1-P65-2	2011年11月
平沢壮, 石原美弥, 藤田真敬, 北垣学, 大谷直樹, 堀口明男, 菊地眞	光音響技術を利用した選択的イメージングの動物モデルによる検証	日本レーザー医学会誌	32(3)	334	2011年10月
石原美弥	光音響画像化技術の最新動向	第3回BioOpto Japan「医療・診断セッション」カンファレンス予稿集		3-1-3-22	2011年9月
Sato M, Ishihara M, Kikuchi M, Mochida J	A diagnostic system for articular cartilage using non-destructive pulsed laser irradiation	Lasers in Surgery and Medicine	43(5)	421-432	2011年7月
Ishihara M, Sato M, Kutsuna T, Mochida J, Kikuchi M	Photoacoustic measurement technology in regenerative medicine of articular cartilage	第50回日本生体医工学学会(CD-ROM)			2011年4月
平沢壮, 石原美弥, 辻田和宏, 入澤覚, 北垣学, 藤	深部組織の高分解能画像化に向けた光音響画像診断法	第50回日本生体医工学会			2011年4月

発表者氏名	論文タイトル名	発表誌名	巻号	ページ	出版年
田真敬, 菊地眞	の開発と評価	(CD-ROM)			

学会発表

発表者氏名	発表タイトル名	学会名	抄録誌名	ページ	発表年
Ishihara M, Hirasawa T, Okawa S, Sato R, Urano Y, Teranishi T	The effect of surface charge of plasmonic gold nanoparticles on photoacoustic signal	SPIE Photonics West Biomedical Optics, BiOS 2014	SPIE Photonics West BiOS 2014 Technical Summaries	305	2014年2月
Okawa S, Hirasawa T, Kushibiki T, Ishihara M	Reconstruction of the optical absorption coefficient from photoacoustic signals measured by scanning coaxial probe with regularization methods	SPIE Photonics West Biomedical Optics, BiOS 2014	SPIE Photonics West BiOS 2014 Technical Summaries	294	2014年2月
Hirasawa T, Okawa S, Fujita M, Kushibiki T, Ishihara M	Quantification of optical attenuation coefficient based on continuous wavelet transform of photoacoustic signals measured by a focused broadband acoustic sensor	SPIE Photonics West Biomedical Optics, BiOS 2014	SPIE Photonics West BiOS 2014 Technical Summaries	326-327	2014年2月
大川晋平, 平沢 壮, 櫛引俊宏, 石原美弥	光音響技術による分子イメージングと光伝播を考慮した定量的画像再構成	第36回日本分子生物学会年会	第36回日本分子生物学会年会要旨集	3AW2-7-3AW2-7	2013年12月
石原美弥	光音響信号の周波数成分が画像性能に与える影響	電気学会光・量子デバイス研究会	電気学会研究会資料 光・量子デバイス研究会 OQD-13-047	27-29	2013年11月
堀口明男, 伊藤敬一, 浅野友彦, 川口真, 辻田和宏, 石原美弥	根治的前立腺全摘術における的確な神経温存のための光音響画像化技術の有用性	第27回日本泌尿器内視鏡学会総会	Japanese Journal of Endourology 26(3)	189	2013年11月
Ishihara M, Okawa S, Sato R, Hirasawa T, Teranishi T	Photoacoustic signal enhancement by localized surface plasmon of gold nanoparticles	Nanomaterials:Application & Properties '2013	Nanomaterials:Application & Properties '2013 Program	43	2013年9月

発表者氏名	発表タイトル名	学会名	抄録誌名	ページ	発表年
石原美弥	光と超音波の特長を併せ持つ光音響断層イメージングの基礎から最先端応用まで	第8回In vivo イメージングフォーラム2013	第8回In vivo イメージングフォーラム2013	16-17	2013年9月
石原美弥	【特別講演】光超音波(光音響)画像診断におけるレーザー安全に関する基礎検討	第1回光超音波画像研究会	第1回光超音波画像研究会プログラム抄録集	1	2013年8月
辻田和宏, 入澤 覚, 広田和弘, 平沢 壮, 藤田真敬, 石原美弥	光音響イメージング装置—光音響画像と超音波画像の融合—	第1回光超音波画像研究会	第1回光超音波画像研究会プログラム抄録集	6	2013年8月
Ishihara M, Hirasawa T, Sato R, Okawa S, Teranishi T	Characterization of photoacoustic signal of plasmonic gold nanoparticles	CLEO-PR & OECC/PS 2013	CLEO-PR & OECC/PS 2013 Conference Program & Abstracts	196	2013年7月
Okawa S, Hirasawa T, Kushibiki T, Ishihara M	Comparison of regularization methods for photoacoustic image reconstruction	Conference on Laser Surgery and Medicine 2013	Proceedings of Conference on Laser Surgery and Medicine 2013	34-35	2013年4月
Okawa S, Hirasawa T, Kushibiki T, Ishihara M	Reconstruction of the optical properties of inhomogeneous medium from photoacoustic signal with lp sparsity regularization	SPIE Photonics West Biomedical Optics, BiOS 2013	SPIE Photonics West BiOS 2013 Technical Summaries	269	2013年2月
Hirasawa T, Fujita M, Okawa S, Kushibiki T, Ishihara M	Improvement in quantifying optical absorption coefficients based on continuous wavelet-transform by correcting distortions in temporal photoacoustic waveforms	SPIE Photonics West Biomedical Optics, BiOS 2013	SPIE Photonics West BiOS 2013 Technical Summaries	289	2013年2月
石原美弥	金ナノ粒子の局在表面プラズモンによる光音	光・量子ビームによるナノダイナミクス			2013年1月

発表者氏名	発表タイトル名	学会名	抄録誌名	ページ	発表年
	響信号増強効果	応用技術調査専門委員会・第2回研究会			
石原美弥	Development of photoacoustic technique towards deeply penetrating in vivo imaging and its clinical application	第35回日本分子生物学会年会	第35回日本分子生物学会年会 プログラム	88	2012年12月
櫛引俊宏, 平沢壮, 大川晋平, 石原美弥	3次元培養細胞観察のための光音響イメージング顕微鏡の創製	第33回日本レーザー医学会	日本レーザー医学会誌 33(3)	318	2012年11月
石原美弥	【特別講演】光音響原理を用いた医療技術の開発:光音響画像の可能	独立行政法人日本学術振興会 生体ひかりイメージング技術と応用185委員会 第2回委員会			2012年10月
大川晋平, 平沢壮, 櫛引俊宏, 石原美弥	光音響信号源分布画像化の逆問題解法によるアプローチ	電気学会 光・量子デバイス研究会	電気学会研究会資料 OQD-12-030	27-31	2012年9月
Ishihara M	【シンポジウム】Photoacoustic imaging and sensing in medicine	14th International Congress of Histochemistry and Cytochemistry	14th International Congress of Histochemistry and Cytochemistry Program and Abstracts	67	2012年8月
Ishihara M, Hirasawa T, Sato R, Teranishi T	Photoacoustic measurements of various gold nanoparticles to design contrast agents for in vivo imaging	XXIV IUPAC Symposium on Photochemistry	XXIV IUPAC Symposium on Photochemistry Abstract book	236	2012年7月
石原美弥	【シンポジウム】「バイオイメージングが医療を変える」光音響原理に基づく組織の分子イメージング	第48回日本小児循環器学会総会・学術集会	日本小児循環器学会雑誌 28(Supplement)	s98	2012年6月
石原美弥	【シンポジウム】光吸収体を超音波で画像化	第7回 日本分子イメージング学会総	日本分子イメージング学会機関誌 5(2)	30	2012年5月

発表者氏名	発表タイトル名	学会名	抄録誌名	ページ	発表年
	する光音響画像:腫瘍診断への可能性	会・学術集会			
櫛引俊宏, 平沢壮, 大川晋平, 石原美弥	光音響技術を用いた in vivo および in vitro 分子イメージングによる生体機能解析	第 5 回医実隊・医大研究交流会			2012 年 5 月
平沢壮, 櫛引俊宏, 藤田真敬, 石原美弥	連続ウェーブレット変換を用いた光音響信号解析による光吸収係数同定法の開発	第 51 回 日本生体医工学会大	生体医工学 50(特別)	212	2012 年 5 月
Kushibiki T, Hirasawa T, Fujita M, Ishihara M	Development and integration of photoacoustic imaging technology	Conference on Laser Surgery and Medicine 2012	Proceedings of Conference on Laser Surgery and Medicine 2012	78-79	2012 年 4 月
Hirasawa T, Ishihara M, Tsujita K, Hirota K, Irisawa K, Kitagaki M, Fujita M, Kikuchi M	Continuous wavelet-transform analysis of photo-acoustic signal waveform to determine optical absorption coefficient	SPIE Photonics West Biomedical Optics, BiOS 2012	SPIE Photonics West BiOS 2012 Technical Summaries	268	2012 年 1 月
Irisawa K, Hirota K, Tsujita K, Hirasawa T, Ishihara M	Influence of laser pulse width to the photoacoustic temporal waveform and the image resolution with a solid state excitation laser	SPIE Photonics West Biomedical Optics, BiOS 2012	SPIE Photonics West BiOS 2012 Technical Summaries	266	2012 年 1 月
平沢壮, 石原美弥, 藤田真敬, 北垣学, 大谷直樹, 堀口明男, 菊地眞	光音響技術を利用した選択的イメージングの動物モデルによる検証	第 32 回日本レーザー医学会総会	日本レーザー医学会誌 32(3)	334	2011 年 11 月
平沢壮, 石原美弥, 藤田真敬, 北垣学, 大谷直樹, 菊地眞	光音響画像化技術の要素技術開発とシステム化:動物モデルによる性能検証	Optics and Photonics Japan 2011	Optics & Photonics Japan 2011	P65-1-P65-2	2011 年 11 月
石原美弥	【特別講演】光音響画像化技術の最新動向	BioOpto Japan 2011	第 3 回 BioOpto Japan 「医療・診断セッショ	3-1-3-2 2	2011 年 9 月

発表者氏名	発表タイトル名	学会名	抄録誌名	ページ	発表年
			ン」カンファレンス予稿集		
石原美弥, 佐藤正人, 沓名寿治, 持田譲治, 菊地眞	【シンポジウム】光音響原理と分光特性を利用した関節軟骨再生の評価	第50回日本生体医工学会大会	生体医工学 49(特別)	197	2011年4月-2011年5月
平沢壮, 石原美弥, 辻田和宏, 入澤覚, 北垣学, 藤田真敬, 菊地眞	深部組織の高分解能画像化に向けた光音響画像診断法の開発と評価	第50回日本生体医工学会大会	生体医工学 49(特別)	311	2011年4月-2011年5月

その他

発表者氏名	タイトル名	発表誌名	巻号	ページ	出版年
石原美弥	光音響法を用いた生体計測技術	光アライアンス	24(9)	12-14	2013年9月
石原美弥	「光音響(光超音波) 画像の最前線②」の特集によせて	日本レーザー医学会誌	34(1)	9	2013年6月
石原美弥	光音響イメージングの最近の進展	日本レーザー医学会誌	34(1)	10-13	2013年6月
石井克典, 橋村圭亮, 北哲也, 粟津邦夫, 近江雅人, 平沢壮, 石原美弥	国際会議報告 Photonics West BiOS 2013	日本レーザー医学会誌	34(1)	50-54	2013年6月
石原美弥	「光音響(光超音波) 画像の最前線」の特集によせて	日本レーザー医学会誌	33(4)	366	2013年1月
櫛引俊宏, 平沢壮, 大川晋平, 石原美弥	低出力レーザーにより引き起こされる生体作用	防衛医科大学校雑誌	37(4)	279	2012年12月
石原美弥	5.バイオメディカルフォトニクスの治療技術応用に関する技術動向 5.1 光音響技術の応用 5.1.1 光音響画像の高分解能化のための画像再構成	電気学会技術報告	1250	46-49	2012年6月
石原美弥	2)光技術動向調査 6.加工・計測 6.5 メディカル応用	OPTOELECTORONICS 2011(平成23)年度 光産業技術に関する報告書		354-359	2012年3月
石原美弥	特集 医師からみた光医療最前線	O Plus E (optics +electronics)	34(2)	122-123	2012年1月
佐藤正人, 石原美弥, 菊地眞, 持田譲治	レーザー・光技術の整形外科領域への応用と展望	O Plus E (optics +electronics)	34(2)	139-144	2012年1月
藤田真敬, 平沢壮, 石原美弥	次世代の画像診断装置としての光音響画像化技術開発と医師の期待	O Plus E (optics +electronics)	34(2)	151-154	2012年1月
平沢壮, 石原美弥, 渡邊智紀, 松浦祐司, 大嶋佑介, 近江雅人, 上野登輝夫, 石井克典, 粟津邦夫	国際会議報告 Photonics West BiOS 2011	日本レーザー医学会誌	32(1)	88-91	2011年6月

V. 研究成果の刊行・別刷

Reconstruction of the optical absorption coefficient from photoacoustic signals measured by scanning coaxial probe with regularization methods

Shinpei Okawa, Takeshi Hirasawa, Toshihiro Kushibiki and Miya Ishihara

Department of Medical Engineering, National Defense Medical College, 3-2 Namiki, Tokorozawa, Saitama, 359-8513, Japan

ABSTRACT

Reconstruction of the absorption coefficient from photoacoustic signals is discussed. The photoacoustic (PA) signals were acquired by using a ring-shaped P(VDF-TrFE) acoustic sensor coaxially arranged with an optical fiber. The acoustic sensor scanned the measured object. The linearized image reconstruction method previously presented by the authors was modified for the measurement with the coaxial probe. The distribution of the absorption coefficient was reconstructed by solving the inverse problem based on the PA wave equation and the photon diffusion equation. The linearized forward model was formulated by solving the partial differential equations with finite element method. To eliminate the effect of the unknown background on the PA signal, the differences between the PA signals measured at different positions were used for the image reconstruction. The image reconstruction method was validated by numerical and phantom experiments. Moreover, the reconstructed images with the Tikhonov and l_p sparsity regularization methods were compared from the standpoints of spatial resolution, robustness to noise and quantification of the absorption coefficient.

Keywords: photoacoustic tomography, P(VDF-TrFE), absorption coefficient, regularization, inverse problem

1. INTRODUCTION

Photoacoustic (PA) imaging[1,2] enables us to diagnose the tissues deep inside the biological medium quantitatively. In PA imaging, nano-second pulse laser illuminates biological tissues, and then the energy of the light absorbed by photon absorber such as hemoglobin is converted into heat. As a result, the thermal expansion of the photon absorber generates elastic wave called PA pressure. The PA pressure depends on the optical absorption coefficients of the photon absorber. Therefore, by calculating the absorption coefficient from the PA signals, quantitative information inside the biological tissue which can be useful for medical diagnoses is obtained.

Although, PA technique images shallow regions because of the limited penetration depth of the excitation light, PA imaging takes advantage of ultrasound imaging and has high spatial resolution from 10 μm to 1 mm. PA signal is not affected by the inhomogeneity of the biological media so much, compared with the light. And also by exploiting the principle of the biomedical measurement using light, PA imaging obtains spectroscopic information which can not be available for ultrasound imaging.

PA image is reconstructed by various techniques. Delay-and-sum backprojection and circular backprojection originally developed for ultrasound imaging can readily be implemented. Frequency-domain reconstruction and universal backprojection which are analytically derived from wave equation were presented by Xu et al.[2] Those analytical reconstruction methods function well in the acoustically homogeneous medium. $k-$space method efficiently calculates the forward solution PA propagation in frequency domain. By using $k-$space pseudospectral methods, Treeby et al reconstructed high-quality image of the vasculature by time-reversal method and compensating the acoustic absorption in acoustically heterogeneous medium.[3]

By taking account of the excitation light propagation, the optical properties and concentrations of the chromophores in optically inhomogeneous medium can be estimated.[4,5] Laufer et al achieved model-based inversion scheme reconstructing the chromophore concentration. This method minimizes the error between the measured and predicted images by using the forward model with photon diffusion equation (PDE) for light propagation and

Shinpei Okawa: E-mail: okawa@ndmc.ac.jp, Telephone: +81 4 2995 1596

Photons Plus Ultrasound: Imaging and Sensing 2014, edited by Alexander A. Oraevsky, Lihong V. Wang,
Proc. of SPIE Vol. 8943, 89433W · © 2014 SPIE · CCC code: 1605-7422/14/$18 · doi: 10.1117/12.2041249

$k-$space method for acoustic wave propagation.[6] Yuan et al reconstructs the optical absorption coefficient using PDE and finite element method (FEM) based PA image reconstruction algorithm.[7] Okawa et al. constructed a linearized reconstruction method based on FEM and numerically investigated the performance.[8]

In this paper, we attempted to reconstruct the distribution of the absorption coefficient from the PA signals acquired by the probe which has coaxially arranged optical fiber to illuminate the measurement object and piezoelectric film to detect PA pressure. The probe scanned the surface of the measured object and measured the PA signals at multiple positions. Then the measured PA signals were used to reconstruct the absorption coefficient. The reconstruction was carried out by solving the inverse problem. The PA forward model was constructed by PA wave equation, and the propagation of the light is taken into account by using PDE. Both equations were solved by FEM. Then the relation between the detected PA signal and the optical properties in the medium was formulated as a linear equation. The image is reconstructed by minimizing the error between the detected and calculated PA signals. In this study, the linearized image reconstruction method previously presented by the authors[9] was modified for the measurement with the coaxial probe. And the differences between the PA signals measured at different positions were used for the reconstruction to eliminate the effect of the unknown background on the PA signals. The numerical and phantom experiments validated the image reconstruction method.

The reconstructed image includes artifacts due to measurement noise and imperfect FEM forward modeling. The ill-posed nature of the inverse problem aggravates the artifacts. A simple forward model, however, is preferable in the sense of the computational cost for practical use. The regularization is one of the useful approaches to reduce the artifacts. The Tikhonov and l_1 sparsity regularizations[9–11] were used in the reconstruction. The regularization methods were compared numerically and experimentally in this study.

2. FORWARD MODELING

2.1 PA pressure propagation

As the nano-second pulse laser illuminates the measured biological medium, the light propagates in the biological medium and is absorbed by the photon absorber such as hemoglobin. And the absorbed light energy is converted into the heat, which generates the PA pressure. When the conditions of the thermal and stress confinements are met, the PA pressure is efficiently generated. The propagation of the PA pressure in an acoustically homogeneous medium is described by the following wave equation,[2]

$$\left\{-\nabla^2 + \frac{1}{v^2}\frac{\partial^2}{\partial t^2}\right\} p(r,t) = \hat{\Gamma}\frac{\partial}{\partial t}H, \tag{1}$$

where v is the speed of the PA pressure p, $\hat{\Gamma}$, Grüneisen parameter associated with the PA efficiency, H, absorbed energy density, and r, the position. The PA source term is the energy of the light absorbed by tissues, which can be calculated by solving following photon diffusion equation. FEM is employed to solve this forward problem in this study.

2.2 Light propagation

The source of the PA signal depends on the distributions of the fluence rate of the light and the absorption coefficient. The absorbed energy density is given by $H = \mu_a\Phi$ with the absorption coefficient μ_a and the fluence rate Φ, which are calculated with PDE.[5] The PA sources are not only diagnostically interesting tissues such as tumor with highly-concentrated blood but also the surrounding normal tissues termed "background" in this study.

The light is scattered and absorbed by biological tissues. The propagation of the excitation light is described by the radiative transfer equation (RTE).[5] In this paper, we use following time-independent PDE which is the approximation of RTE,

$$\{-\nabla \cdot D(r)\nabla + \mu_a(r)\}\,\Phi(r) = q_0(r), \tag{2}$$

where D is the diffusion coefficient, μ_a, the absorption coefficient, Φ, the fluence rate of light, q_0, the light source. PDE is hold when the medium is thick enough and the time after the pulse light incidence is longer. The

boundary condition is given as $-n \cdot D\nabla\Phi = 1/(2A)\Phi$ where n is the vector normal to the surface of the medium, and A is the parameter depending on the internal reflection ratio. PDE can be solved by using FEM.

2.3 Forward formulation for reconstruction from measurements with coaxial probe

The PA signal is measured by the probe which has the coaxially arranged optical fiber as the light source and piezoelectric film as the detector. That means that the illuminating and detecting positions are identical. Let us assume that the probe illuminates the light at the upper surface of the measured object and that the detector has high directivity and is sensitive to the PA pressure generated by the PA sources located directly below the coaxial probe. Equation (1) indicates that the detected PA signal is linearly related with the PA source term. Therefore, following linear equation relates the PA signals measured at k-th position to the PA sources just below the probe,

$$\boldsymbol{m}_k = L_k \boldsymbol{H}_k, \tag{3}$$

where $\boldsymbol{m}_k$ is a T-vector of the set of PA signals with T time samples measured by the coaxial probe at k-th position, and $\boldsymbol{H}_k$ is an M-vector of the PA source below the probe spatially discretized into M pixels. L_k is a $T \times M$-matrix representing the contributions of the discretized sources to the measured signals. L_k is obtained by calculating PA signals generated by each of the sources with a unit strength.

$\boldsymbol{H}_k$ is described as a first-order Talor expansion about the background absorption coefficient $\bar{\mu}_a$. Then, Eq.(3) is rewritten to relate $\boldsymbol{m}_k$ and μ_a as,

$$\boldsymbol{m}_k = L_k \left(\bar{\boldsymbol{H}}_k(\bar{\mu}_a) + J_k \Delta\mu_a \right), \tag{4}$$

where $\bar{\boldsymbol{H}}_k$ is the PA source generated by the background absorption and $\Delta\mu_a$ is an N-vector of the distribution of the perturbation of μ_a in the whole of medium discretized into N pixels. J_k is the matrix consists of the differential coefficients of $\boldsymbol{H}_k$ at $\bar{\mu}_a$ and is calculated by perturbation method using FEM with Eq.(2).

In this study, we attempt to reconstruct $\Delta\mu_a$. The large change in μ_a can indicate the diseased tissue such as cancer with angiogenesis. The difference between PA signals measured at different two positions are used for the reconstruction to eliminate the effect of the unknown $\bar{\mu}_a$ on PA signals. By assuming that the medium is so large that the baundary effect on the measurement is negligible, $L_k \bar{\boldsymbol{H}}_k \simeq L_l \bar{\boldsymbol{H}}_l$, $(k \neq l)$. Then we obtain,

$$\begin{aligned} \Delta\boldsymbol{m}_{k,l} &= \boldsymbol{m}_k - \boldsymbol{m}_l \\ &= \left(L_k J_k - L_l J_l \right) \Delta\mu_a \\ &= G_{k,l} \Delta\mu_a. \end{aligned} \tag{5}$$

The reconstruction of $\Delta\mu_a$ is conducted with the following forward equation,

$$\Delta\boldsymbol{m} = G\Delta\mu_a, \tag{6}$$

where $\Delta\boldsymbol{m}$ is the vector consists of $\Delta\boldsymbol{m}_{k,l}$, and G is the matrix consists of $G_{k,l}$.

In this study, the detected PA signals and the matrix G were down-sampled to reduce the calculation cost for efficient reconstruction. Considering the pixel size, it is not necessary to use all temporal samples of the PA signal. We sampled the datum which had the maximum absolute value of the PA signal in every interval of 0.133 μs (= 2 mm / 1.5 mm $\cdot$ μs^{-1}) as the signal for the reconstruction under the assumption that the signal-to-noise ratio was sufficiently high.

3. IMAGE RECONSTRUCTION

3.1 Reconstruction with Tikhonov regularization

The reconstruction of $\Delta\mu_a$ is carried out by solving the optimization problem with the Tikhonov regularization,[10]

$$\min_{\Delta\mu_a} \left\| \Delta\boldsymbol{m} - G\Delta\mu_a \right\|^2 + \lambda \cdot \left\| \Delta\mu_a \right\|^2, \tag{7}$$

where $\Delta\boldsymbol{m}$ is composed of the PA signals measured at multiple positions and λ is a regularization parameter to adjust the effect of the regularization term on the reconstruction. Then the reconstructed $\widehat{\Delta\mu_a}$ is obtained as,

$$\widehat{\Delta\mu_a} = \left(G^T G + \lambda \cdot I \right)^{-1} G^T \Delta\boldsymbol{m}. \tag{8}$$

3.2 Reconstruction with l_p sparsity regularization

A sparse solution is obtained by using the l_p sparsity regularization[11] which minimizes the p-norm of the solution with the residual error. The spatial resolution of the reconstructed image with l_p sparsity regularization is higher than that with the Tikhonov regularization.[9,11] The image reconstruction with the l_p sparsity regularization in this study is described as follows,

$$\min_{\Delta\mu_a} \|\Delta \boldsymbol{m} - G\Delta\mu_a\|^2 + \lambda \cdot f(\Delta\mu_a), \tag{9}$$

where f is a regularization term and λ is a regularization parameter.

l_p sparsity regularization employs f of the p-norm of $\Delta\mu_a$,

$$f = \sum_{i=1}^{M} |\Delta\mu_{a_i}|^p, \tag{10}$$

where $0 < p \leq 2$. When $p \leq 2$, it is problematic to calculate the gradient of f for non-linear gradient based optimization. So, $\Delta\mu_{a_i}$ is expressed by a parameter z_i,[11]

$$\Delta\mu_{a_i} = |z_i|^{2/p} \cdot \mathrm{sgn}(z_i). \tag{11}$$

Then the optimization problem Eq.(6) is rewritten as,

$$\min_{\boldsymbol{z}} \|\Delta \boldsymbol{m} - G\Delta\mu_a(\boldsymbol{z})\|^2 + \lambda \cdot \sum_{i=1}^{M} |z_i|^2. \tag{12}$$

By solving the optimization problem in Eq.(9), $\widehat{\Delta\mu_a}$ is reconstructed. It is expected that the l_p sparsity regularization with $p < 2$ provides a sparse solution, and the spatial resolution of the reconstructed image is improved. $p = 1$ was used in this study.

4. CONDITIONS OF NUMERICAL SIMULATION AND PHANTOM EXPERIMENT

4.1 Numerical simulation

In the numerical simulation, the spatial resolution and the quantification ability of the reconstructions with the Tikhonov regularization and the l_p sparsity regularization were compared.

Figure 1(a) shows 2D geometry used in the numerical simulations. The medium was a square region with 50 mm side. The illuminating and detecting positions were identical. The PA signals were measured at 11 positions of $x = -10, -8, \cdots, 10$ mm on $y = 0$ mm. The light source with a wavelength in NIR range was assumed, and the optical properties of the background medium are uniformly distributed with $\bar{\mu}_s' = 0.8$ mm^{-1} and $\bar{\mu}_a = 0.01$ mm^{-1}. The target, which had μ_a larger than that of the background, was placed in the medium. The position of the target was y =20 or 18 mm on $x = 0$ mm. The target was a circle with 1 mm diameter. The reconstructions were conducted when the target had μ_a of 0.1, 0.2, 0.5 or 1.0 mm^{-1}. We attempted to reconstruct $\Delta\mu_a$ by the Tikhonov and the l_p sparsity regularizations.

FEM was used with 10,201 nodes and 20,000 triangular elements to simulate PA signals. The FEM nodes were distributed uniformly with an equal spacing of 0.5 mm. The speed of the PA pressure in the medium of 1.5 mm/μs was used for the FEM calculation, and Grüneissen parameter was set as unity. The time-dependent terms in eq.(2) was calculated by differential approximation with time step of $\Delta t = 0.1$ μs. Equation (2) discretized by FEM was solved with implicit scheme. We assumed that measurement period was 50 μs.

We carried out the image reconstruction on pixel basis. The medium was discretized into 625 pixels. Every pixel with 2 mm side contained 25 FEM nodes. The PA signals generated by the sources at FEM nodes in a single pixel was averaged and was used as the contribution (a single column of the matrix L_k) of a single-pixel PA source to the measurement data. The component of J_k was also the average over the nodes in a single pixel. The regularization parameter was selected empirically.

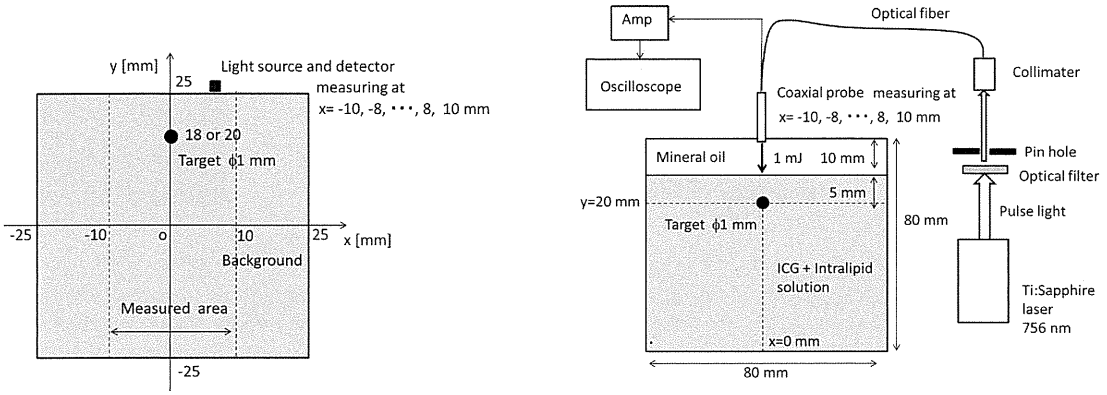

Figure 1. (a) 2D geometries for numerical simulation and (b) Schematic chart of the phantom experiment.

4.2 Phantom experiment

The improvement in localization of the target reconstructed by the l_p sparsity regularization was demonstrated by comparing the Tikhonov regularization in the phantom experiment.

Figure 1(b) illustrates the schematic chart of the phantom experiment. A tunable Ti:sapphire laser (LT-2211, Lotis Tii, Minsk, Belarus) pumped by the second harmonic of a Q-switched Nd:YAG laser (LS-2134, Lotis Tii, Minsk, Belarus) was used to produce excitation light pulses with a width of about 10 ns and a repetition frequency of 15 Hz at 756 nm. The light pulse was coupled into a multi-mode optical fiber (M41L02, Thorlabs, Newton, NJ) with a core diameter of 0.6 mm. The optical fiber was introduced into a cylindrical probe which had a ring shaped piezoelectric film P(VDF-TrFE) (KF piezo-film, Kureha Corp., Tokyo, Japan) on the detecting surface. The film had a thickness of 20 μm. The edge of the optical fiber, from which the light pulse of 1 mJ was emitted, was located at the center of the film, and the light source and the detector were coaxially arranged. The detected PA signal was amplified by the noise field-effect transistor amplifier (SA-220FS, NF Electronic Instruments, Yokohama, Japan), and recorded by a digital oscilloscope (DSO7104A, Agilent Technologies, Santa Clara, CA). The PA signals were averaged over 100 light pulses online. The sampling rate was 20 MHz. $\Delta\mu_a$ was processed with offline lowpass filter with a cutoff frequency of 4.6 MHz. The image reconstructions were conducted with the same manner in the numerical simulation.

The measured object was a liquid phantom made of intralipid and indocyanine green (ICG) diluted with water. The optical properties of the phantom was adjusted to $\mu_s' = 0.8$ mm^{-1} and $\mu_a = 0.01$ mm^{-1}. There existed a target in the phantom. The target was a polybutadien tube containing diluted intralipid and ICG. The optical properties of the target were $\mu_s' = 0.8$ mm^{-1} and $\mu_a = 0.62$ mm^{-1}.[12]

5. RESULTS AND DISCUSSIONS

5.1 Numerical simulation

The reconstructed images when the true target was at $(x,\ y) = (0$ mm, 18 mm$)$ are shown in Fig. 2(a) and (b). The Tikhonov regularization reconstructed maximum of $\widehat{\Delta\mu_a}$ at the true position of the target. However, the distribution of $\Delta\mu_a$ broadened and the target was reconstructed at the correct position and the pixels at neighboring to the true position. The Tikhonov regularization provides the smooth solution. Therefore, it is difficult to obtain sparse high resolved image with the Tikhonov regularization. The maximum of $\widehat{\Delta\mu_a}$ was about 1.2×10^{-3} mm^{-1}.

On the other hand, by the l_p sparsity regularization, the target was reconstructed in a single pixel at the true position of the target as shown in Fig. 2(b). The maximum of $\widehat{\Delta\mu_a}$, about 0.04 mm^{-1}, was 4 times larger than that reconstructed by the Tikhonov regularization. By localizing the PA source in a small area, the strength of the PA source became larger.

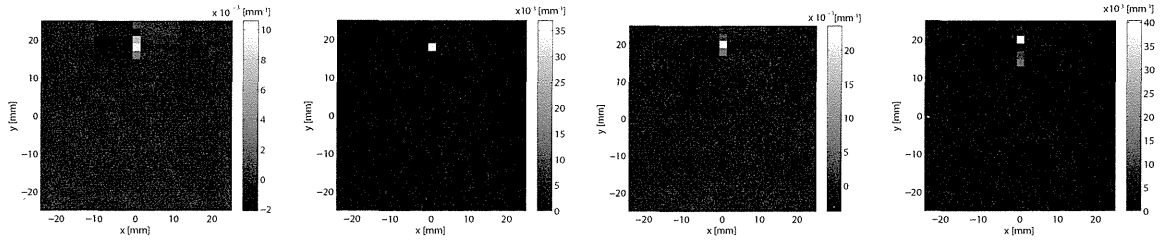

Figure 2. The reconstructed images with (a) theTikhonov and (b) the l_p sparsity regularizations when the true target was at $(x,\ y) = (0\text{ mm},\ 18\text{ mm})$ and with (c) the Tikhonov and (d) the l_p sparsity regularizations when the true target was at $(x,\ y) = (0\text{ mm},\ 20\text{ mm})$ in the numerical simulation.

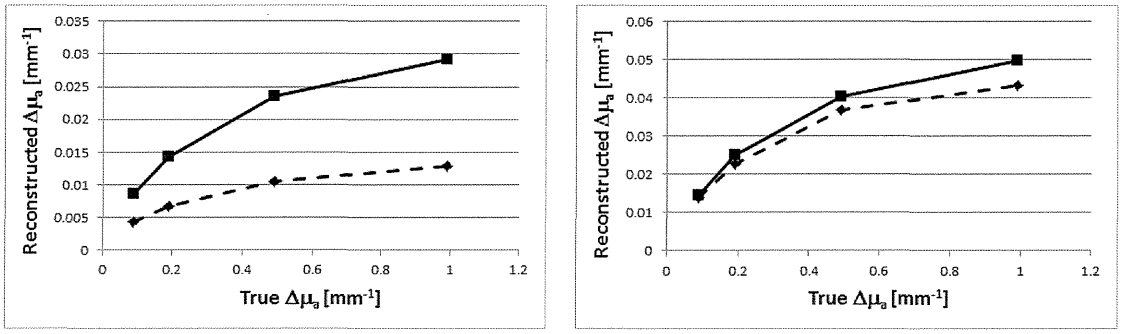

Figure 3. The reconstructed $\Delta\mu_a$ with (a) the Tikhonov and (b) the l_p sparsity regularizations as a function of true $\Delta\mu_a$ when the true target was at $(x,\ y) = (0\text{ mm},\ 18\text{ mm})$ (dashed line) or $(x,\ y) = (0\text{ mm},\ 20\text{ mm})$ (solid line).

The target reconstructed at the correct position by the Tikhonov regularization was well localized when the true target was at $(x,\ y) = (0\text{ mm},\ 20\text{ mm})$. The l_p sparsity regularization increased the value of $\widehat{\Delta\mu_a}$. The reconstructed value of $\widehat{\Delta\mu_a}$ was much smaller than true one, because the pixel size was larger than the target size and the reconstructed $\widehat{\Delta\mu_a}$ was deconcentrated. The regularizations were also causes of the underestimation of the $\widehat{\Delta\mu_a}$. The smaller the reconstructed values, the smaller the regularization terms in Eqs.(7) and (12).

Figure 3(a) shows the maximum of $\widehat{\Delta\mu_a}$ with the Tikhonov regularization as a function of true $\Delta\mu_a$. Although the true $\Delta\mu_a$ was same, $\widehat{\Delta\mu_a}$ in $y = 18$ mm was smaller than that in $y = 20$ mm when the reconstruction was carried out with the Tikhonov regularization. That was because the reconstructed target at $y = 18$ mm broadened more than that at $y = 20$ and the strength of the PA source was deconcentrated. Although decreasing Φ owing to the scattering and the absorption by the medium was taken into account for the reconstruction by employing PDE, $\widehat{\Delta\mu_a}$ depended on the depth from the surface. It is difficult to quantify the absorption coefficient because of the nature of the inverse problem.

By localizing $\widehat{\Delta\mu_a}$ by using the l_p sparsity regularization and by alleviating the deconcentration, the difference between the reconstructed targets at $y = 18$ mm and $y = 20$ mm became smaller as shown in Fig. 3(b). The quantitative ability of the image reconstruction was improved by the l_p sparsity regularization. The relative error between $\widehat{\Delta\mu_a}$ at $y = 18$ and $y = 20$ mm were decreased from about 32 % to 1%. The reconstructed $\widehat{\Delta\mu_a}$ did not linearly depend on the true values. The linearization in the forward modeling implied that $\Delta\mu_a$ was small. Therefore, the large changes in μ_a were not reconstructed correctly by the linearized reconstruction method.

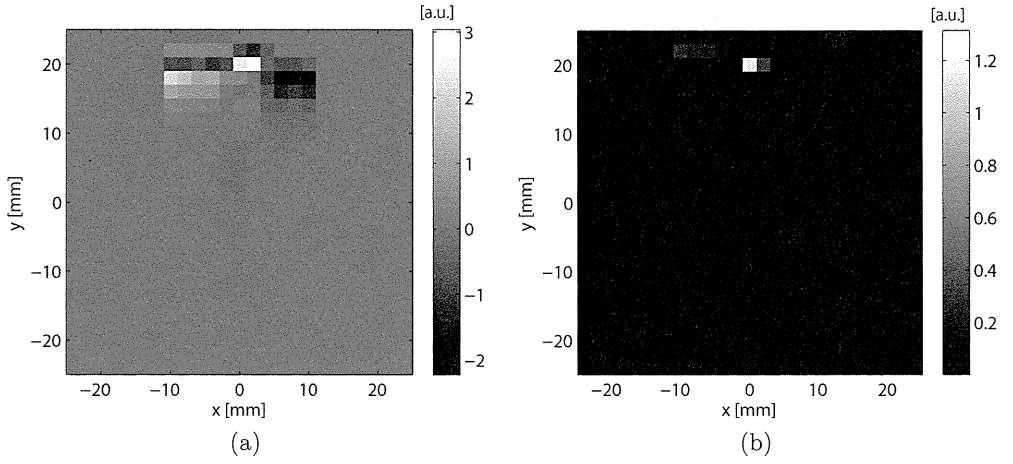

Figure 4. The reconstructed images with (a) the Tikhonov and (b) the l_p sparsity regularizations when the true target was at $(x,\ y) = (0\text{ mm},\ 20\text{ mm})$.

5.2 Phantom experiment

Figure 4 shows the reconstructed images in the phantom experiment. The target at $(x,\ y) = (0\text{ mm},\ 20\text{ mm})$ is found in the image reconstructed by the Tikhonov regularization in Fig. 4(a). The reconstruceted target was broadened and astride the two pixels. One of the possible reasons was the real detector did not have the ideal high directivity and detected the PA signals from the PA sources which was not directly below the detector. Noise caused the artifacts in the reconstructed image.

On the other hand, the target was clearly reconstructed by the l_p sparsity regularization. Although some small artifacts can be seen in the reconstructed image in Fig. 4(b), the target reconstructed by the l_p sparsity regularization was localized more than that by the Tikhonov regularization. $\widehat{\Delta\mu_a}$ with the l_p sparsity regularization did not become larger than that with the Tikhonov regularization in the phantom experiment. Measurement noises and the selection of the regularization parameter might make the differences between the phantom experiment and the numerical simulation.

The improvement in localization of the target reconstructed by the l_p sparsity regularization was successfully demonstrated by the phantom experiment. To investigate the effects of the l_p sparsity regularization on the PA image reconstruction experimentally, more precise experiments may be needed.

6. CONCLUSION

The reconstruction of the optical coefficient from the photoacoustic signals measured by a coaxial probe was tried in this study. The probe had a ring shaped P(VDF-TrFE) film to detect the acoustic signal and the optical fiber to illuminate the measured object coaxially. By eliminating the PA signals generated by the background, the changes in the absorption coefficient were reconstructed by solving the linearized inverse problem in the numerical simulation and phantom experiment. The Tikhonov and l_p sparsity regularizations were used and compared. The l_p sparsity regularization improved the localization of the reconstructed target in the numerical simulation and the phantom experiment. It was shown in the numerical simulation that the quantification ability of the reconstructed target was also improved.

ACKNOWLEDGEMENTS

This work was supported in part by JST Collaborative Research Based on Industrial Demand (In vivo Molecular Imaging: Towards Biophotonics in Medicine) and JSPS KAKENHI Grant Number 24760314. Finally, we would like to acknowledge Hiroaki Ishihara for assisting us in the phantom experiment.

REFERENCES

[1] L. V. Wang and S. Hu, "Photoacoustic Tomography: In Vivo Imaging from Organelles to Organs," *Science*, **335**, pp. 1458-1462, 2012.

[2] M. Xu and L. V. Wang, "Photoacoustic imaging in biomedicine," *Rev. Sci. Instrum.*, **77**, pp. 041101-1-22, 2006.

[3] B. E. Treeby, E. Z. Zhang and B. T. Cox, "Photoacoustic tomography in absorbing acoustic media using time reversal," *Inverse Probl.*, **.26**, pp. 115003-115023, 2010.

[4] B. Cox, J. G. Laufer, S. R. Arridge and P. C. Beard "Quantitave spectroscopic photoacoustic imaging: a review," *J. Biomed. Opt.*, **17**, pp. 061202-1-22, 2012.

[5] S. R. Arridge, "Optical tomography in medical imaging," *Inverse Probl.*, **15**, pp. R41-R93, 1999.

[6] J. Laufer, B. Cox, E. Zang and P. Beard, "Quantitative determination of chromophore concentrations from 2D photoacoustic images using a nonlinear model-based inversion scheme," *Appl. Opt.*, **49**, pp.1219-1233, 2010.

[7] Z. Yuan, Q. Wang and H. Jiang, "Reconstrcution of optical absorption coefficient map of heterogeneous media by photoacoustic tomography coupled with diffusion equation based regularized Newton method," *Opt. Express*, **15**, pp.18076-18081, 2007.

[8] S. Okawa, T. Hirasawa, T. Kushibiki and M. Ishihara, "Numerical evaluation of linearized image reconstruction based on finite element method for biomedical photoacousitc imaging," *Opt. Rev.*, **20**(5), pp. 442-451, 2013.

[9] S. Okawa, T. Hirasawa, T. Kushibiki and M. Ishihara, "Reconstruction of the optical properties of inhomogeneous medium from photoacoustic signal with l_p sparsity regularization," *Proc. SPIE*, **8581**, 858135, 2013.

[10] C. R. Vogel, Computational Methods for Inverse Problems, The Society of Industrical and Applied Mathematics, 2002.

[11] S. Okawa, Y. Hoshi and Y. Yamada, "Improvement of image quality of time-domain diffuse optical tomography with l_p sparsity regularization," *Biomed. Opt. Express*, **2**(12), pp. 3334-3348, 2011.

[12] H. J. van Staveren, C. J. M. Moes, J. van Marie, S. A. Prahl and M. J. C. van Gemert, "Light scattering in Intralipid-10% in the wavelength range of 400-1100 nm," *Appl. Opt.*, **30**(31), pp. 4507-4514, 1991.